

# Monotropein alleviates sepsis-associated encephalopathy by targeting matrix metalloproteinase-9

Yue Xin<sup>a,b,1</sup>, Tianyue Guan<sup>a,b,1</sup>, Guanglu Wang<sup>a,b,1</sup>, Yannan Xiang<sup>a,b</sup>, Mengxin Li<sup>a,b</sup>, Yikun Zhao<sup>a</sup>, Panpan Zhao<sup>a,\*</sup>

<sup>a</sup> Institute of Neuroscience, Neurosurgery Department, The First People's Hospital of Lianyungang, Lianyungang, 222000, China

<sup>b</sup> Jiangsu Key Laboratory of Marine Pharmaceutical Compound Screening, College of Pharmacy, Jiangsu Ocean University, Lianyungang, 222005, China

## ARTICLE INFO

### Keywords:

Monotropein  
Sepsis-associated encephalopathy  
CLP  
MMP9  
Brain tissue damage  
Oxidative stress

## ABSTRACT

Sepsis is a severe systemic infection that leads to multiple organ dysfunction and high mortality, making it one of the primary causes of death in ICU patients. Sepsis also induces septic encephalopathy (SAE), resulting in acute and long-term cognitive impairments. Research indicates that inhibiting BBB damage, anti-inflammatory, and antioxidant responses are critical therapeutic directions for SAE. Monotropein (Mon), the main active component of the traditional Chinese medicine Epimedium, possesses various pharmacological effects, including antioxidant properties. This study aims to explore the protective effects and potential targets of Mon in SAE. Firstly, the GEO database was utilized to screen for highly expressed genes, identifying matrix metalloproteinase-9 (MMP9) as a target. Drug target reverse screening using Schrodinger software confirmed MMP9 as a potential therapeutic target for Mon. Subsequently, *in vitro* experiments using an LPS-stimulated BV-2 and HUVECs co-culture model examined the interaction between Mon and MMP9. A CLP-induced mouse model was employed to investigate Mon's role in SAE. Results indicate that MMP9 is highly expressed in SAE and promotes its progression. Mon targets MMP9, enhancing its protein stability and exerting anti-inflammatory, improved vascular permeability, and barrier protective effects. Mon alleviates brain tissue damage, BBB disruption, and synaptic loss induced by CLP, increases antioxidant enzyme activity to eliminate ROS, and suppresses sepsis-induced oxidative stress, thereby mitigating CLP-induced cognitive impairment in mice. In conclusion, Mon targets MMP9, exerting anti-inflammatory, antioxidant, and barrier protective effects, alleviating SAE. Mon may serve as a potential natural therapeutic agent for treating sepsis-induced brain dysfunction.

## 1. Introduction

During sepsis, systemic inflammation affects the brain through complex pathways, leading to sepsis-associated encephalopathy (SAE). SAE manifests as diffuse brain dysfunction in septic patients without direct CNS infection or structural abnormalities (Manabe and Heneka, 2022; de Araújo et al., 2022). Symptoms range from altered perception to coma, affecting behavior, cognition, and consciousness (Piva et al., 2023). Long-term cognitive impairments are common, with a high incidence (up to 70 %) and elevated mortality rates in critically ill patients with SAE (Ito et al., 2022; Catarina et al., 2021). Factors like inappropriate antimicrobial use contribute to neurotransmitter imbalances, influencing SAE onset (Dumbuya et al., 2023). Sepsis disrupts the

blood-brain barrier, triggering inflammation, oxidative stress, and impairing CNS neurotransmission and cerebral circulation (Q. Gao and Hernandez, 2021; H.R. Li et al., 2023). Strategies targeting BBB protection, anti-inflammatory actions, and oxidative stress mitigation are crucial for SAE treatment.

Matrix metalloproteinase-9 (MMP9) is a crucial enzyme in the matrix metalloproteinase family, essential for maintaining extracellular matrix dynamics (Augoff et al., 2022). It plays pivotal roles in various physiological and pathological processes, including immune-related diseases of the central nervous system (CNS), thrombolytic therapy for stroke, and research on blood-brain barrier (BBB) integrity (Hu et al., 2024; Kaczmarek et al., 2023; Ringland et al., 2021). The BBB, formed by brain capillary walls and glial cells, protects the brain by selectively allowing

\* Corresponding author.

E-mail addresses: [xinyueyue@163.com](mailto:xinyueyue@163.com) (Y. Xin), [guantianyue0211@163.com](mailto:guantianyue0211@163.com) (T. Guan), [2021226066@jou.edu.cn](mailto:2021226066@jou.edu.cn) (G. Wang), [lygxyn@163.com](mailto:lygxyn@163.com) (Y. Xiang), [2023221045@jou.edu.cn](mailto:2023221045@jou.edu.cn) (M. Li), [zyklygy@outlook.com](mailto:zyklygy@outlook.com) (Y. Zhao), [zhaopp19@mails.jlu.edu.cn](mailto:zhaopp19@mails.jlu.edu.cn) (P. Zhao).

<sup>1</sup> These authors contributed equally to this study.

<https://doi.org/10.1016/j.neuropharm.2025.110636>

Received 14 December 2024; Received in revised form 30 July 2025; Accepted 11 August 2025

Available online 12 August 2025

0028-3908/© 2025 Published by Elsevier Ltd.

nutrients and small molecules while blocking harmful substances (Peng et al., 2021; Simões Da Gama and Morin-Brureau, 2022). MMP9's involvement in BBB damage is well-documented in CNS immune diseases. It degrades essential components like basement membranes and tight junctions, critical for BBB integrity (Ji et al., 2023). For example, MMP9 can break down tight junction proteins, compromising barrier function. Studies suggest that in CNS immune diseases such as multiple sclerosis, activated microglia regulate BBB integrity via the MiR-126a-5p/MMP9 axis, influencing disease progression (Yan et al., 2022; Yu et al., 2022). Chronic arsenic exposure or aging can elevate MMP9/2 levels, contributing to BBB tight junction disruption (Lv et al., 2023). MMP9 levels in serum and cerebrospinal fluid also impact BBB integrity in CNS infections (Dal-Pizzol et al., 2013). MMP9's ability to degrade BBB components and its activation in inflammatory responses make it a significant therapeutic target for CNS immune diseases.

Monotropein (Mon) is a compound derived from plants like *Symphytum officinale* and *Morinda officinalis*, belonging to the cyclohexane terpenoid glycoside group (Z. Li, Li et al., 2023; Shin et al., 2013). It's a major active component of traditional Chinese medicine, known for diverse biological activities (Wu et al., 2023; Mieres-Castro et al., 2019). Mon exhibits anti-inflammatory, antioxidant, antimicrobial, and anti-tumor effects (Guo et al., 2024; C. Wang et al., 2018). Studies highlight its role in colorectal cancer treatment by modulating inflammation-related pathways (Lu et al., 2023). Mon enhances antioxidant enzyme activities and reduces oxidative stress markers like MDA (Y. Zhang et al., 2020). It also protects cells from oxidative damage and mitochondrial dysfunction (F. Jiang et al., 2020). These properties suggest Mon's potential in food and pharmaceutical applications, particularly in treating sepsis-related brain damage.

This study aims to investigate the potential therapeutic effects of Mon on SAE. The research involves establishing both an *in vivo* mouse model of cecal ligation and puncture (CLP) and an *in vitro* model using co-cultures of BV-2 and HUVECs stimulated with LPS. The study analyzes the pathological role of MMP9 in sepsis-induced BBB damage and explores Mon's targeted effects on MMP9, as well as its various biological activities such as anti-inflammatory and antioxidant properties. This research aims to expand the pharmacological functions of Mon and provide new insights for the development of therapeutic strategies for SAE in the future.

## 2. Methods

### 2.1. Experimental animals and experimental design

Male BALB/c mice (20–25 g, 6 weeks old) were purchased from Yangzhou University's Experimental Animal Center. After a 7-day acclimatization in controlled conditions ( $55 \pm 15$  % humidity,  $25 \pm 2$  °C temperature) with free access to food and water. All procedures followed the "Principles of Care for Laboratory Animals" (NIH Publication No. 85-23, amended in 1985), and the Animal Ethics Committee of Jiangsu Ocean University approved the animal experiments of this study (license number: 2022221092).

The experimental animals were randomly divided into the following six groups, with 6 mice in each group: Control Group: This group represents the untreated animals, serving as a baseline for comparison. Sham Group: Mice underwent laparotomy after anesthesia and were sutured immediately without any drug treatment. Sham + Mon Group: Mice underwent sham surgery and received intraperitoneal injections of Mon (20 mg/kg BW) (Guo et al., 2024) for 4 consecutive days. CLP Group: Mice underwent cecal ligation and puncture surgery after anesthesia. CLP + Mon Group: Mice received intraperitoneal injections of Mon (20 mg/kg BW) (Guo et al., 2024) for 4 consecutive days after surgery. CLP + Dex Group: Mice received intraperitoneal injections of DEX (2 mg/kg BW) (Shi et al., 2021) for 4 consecutive days after surgery.

### 2.2. CLP model

The CLP procedure was done as described (Sun et al., 2020). Mice were anesthetized with 100 mg/kg of ketamine intraperitoneally. The cecum was ligated with 4.0 silk suture, punctured with a 21 G needle, and a small amount of feces was extruded. The cecum was then returned to the abdominal cavity and sutured. Mice received 0.1 mL of pre-warmed saline subcutaneously for resuscitation. Sham-operated mice had the same procedure without ligation and puncture. Five days later, brain tissues were collected for Western blotting and biochemical assays (12 mice per group), and behavioral testing was performed (3 mice per group).

After surgery, the mice were placed on a thermostatic heating pad and resuscitated with an intraperitoneal injection of normal saline. They were then allowed free access to food and water. All procedures were strictly performed in accordance with the Principles of Care for Laboratory Animals to ensure animal welfare.

### 2.3. Cell culture

Human Umbilical Vein Endothelial Cells (HUVECs) and BV-2 cells (murine microglial cells) were cultured in high-glucose DMEM complete medium at 37 °C with 5 % CO<sub>2</sub>.

### 2.4. Drug administration

Monotropein (Mon, CAS# 5945-50-6, HPLC  $\geq 98$  %, Aladdin, Shanghai) was dissolved in DMSO (Sigma, USA, CAS# 200-664-3). Following CLP surgery, mice in the CLP and sham-operated groups received daily intraperitoneal injections of 20 mg/kg body weight (BW) Mon for 4 consecutive days (Guo et al., 2024). The positive control group received dexamethasone (DEX, 2 mg/kg BW) (Shi et al., 2021). In cell experiments, BV-2 and HUVECs were treated with LPS (1 µg/mL) for 24 h (Hou et al., 2019). Mon was administered to cells at a concentration of 100 µM for 24 h firstly (F. Jiang et al., 2020). Then MMP9-IN-1 (100 µM) was used to pretreat cells for 2 h (Dufour et al., 2011), followed by stimulation with 1 µg/mL LPS for 24 h.

### 2.5. BBB detection

BV-2 cells were seeded at a density of  $1 \times 10^5$  cells per square centimeter in 24-well cell culture plates. The following day, HUVECs were seeded at a density of  $1.5 \times 10^5$  cells per square centimeter on Transwell inserts with a pore size of 0.4 µm (Nunc, Thermo Scientific Inc, USA) and placed in a cell culture incubator for further cultivation. To evaluate the integrity of the blood-brain barrier (BBB) *in vitro*, tight junction protein expression, including ZO-1, Occludin, and Claudin-5, was analyzed by Western blotting. For *in vivo* assessment of BBB permeability, Evans Blue dye was administered intravenously, and brain tissue was collected for cryosectioning. BBB disruption was subsequently visualized and quantified based on Evans Blue staining of the frozen brain sections.

### 2.6. TEER measurement

TEER of HUVECs co-cultured with BV-2 cells was measured using the Millicell-ERS system (Millipore, USA) to assess barrier integrity. First, the electrodes should be equilibrated in DMEM/F12 culture medium for up to 24 h. This step allows full contact between the electrodes and the culture medium, ensuring stability and consistency during measurement. Following equilibration, the electrodes must undergo a rigorous disinfection process to prevent potential contamination that could interfere with the results. The electrodes are immersed in 75 % alcohol for 15 min, which effectively eliminates bacteria and other microorganisms. After disinfection, the electrodes are removed and left at room temperature for 1 min to air dry, preventing any residual alcohol from

affecting the subsequent experiments. Once disinfected and dried, the electrodes are then placed in buffer solution for an additional 15-min equilibration period. During resistance measurement, it is essential to thoroughly measure each well and record the resistance value ( $R_t$ ). To ensure reliability, each well is measured at least three times, and the average value is calculated. At the same time, the resistance of blank wells (without cells) is also recorded as control values ( $R_o$ ), which is used for TEER calculation.

The TEER is calculated using the formula:  $TEER = (R_t - R_o) \times S$ , where  $S$  represents the effective membrane area. This calculation provides the transendothelial electrical resistance, which reflects the integrity and functional status of the cell monolayer.

## 2.7. Gene expression omnibus (GEO) database

The GEO database (<https://www.ncbi.nlm.nih.gov/geo/>) was utilized to analyze differential gene expression related to sepsis-associated encephalopathy (SAE). Dataset GSE167610 was selected for the study of sepsis-associated brain disease. Differential gene expression analysis was performed using the GEO2R tool, with the screening criteria set as  $P < 0.05$  and  $|\log FC| > 0$ .

## 2.8. Immunofluorescence staining

BV-2 cells were stained for Iba-1 (1:1000, Servicebio, Wuhan) and MMP9 (1:800, Proteintech, Wuhan) expression using confocal microscopy.

## 2.9. Western blotting

Proteins from six-well plates or brain tissues were extracted using RIPA lysis buffer. After centrifugation, supernatants were collected, and protein concentrations were measured with a BCA assay kit. Proteins were separated by SDS-PAGE, transferred to PVDF membranes, and blocked. Membranes were then incubated with primary antibodies overnight, followed by secondary antibodies. Protein bands were visualized using ECL chemiluminescence and quantitatively analyzed with ImageJ software.

The primary antibodies used were obtained from Proteintech, Wuhan, China: GAPDH (60004-1-Ig, 1:50000), Bax (50599-2-Ig, 1:20000), MMP9 (27306-1-AP, 1:1000). The primary antibodies against Bcl-2 (WL01556, 1:1000), Caspase 3 (WL02117, 1:1000) were purchased from Wanleibio Co., Ltd., Shenyang, China. Secondary antibodies included anti-rabbit IgG (SA00001-2, 1:2000) and anti-mouse IgG (SA00001-1, 1:2000), both from Proteintech, Wuhan, China.

## 2.10. H&E staining

Brain tissue sections were stained to observe pathological changes under an optical microscope (Leica, Japan).

## 2.11. Transmission electron microscopy (TEM) experiment

Brain tissue samples were fixed overnight in 4 % glutaraldehyde fixative (BL912A, Biosharp), dehydrated in acetone, embedded in resin, and polymerized at high temperature. Thin sections (70 nm) were cut using an ultramicrotome, stained with uranyl acetate and lead citrate, dried, mounted on carbon-coated copper grids, and observed using TEM (Hitachi H-7650).

## 2.12. Biochemical assays

Samples were homogenized using a high-throughput tissue grinder at low temperature. For general analysis, tissue was homogenized in a 1:9 ratio with physiological saline (v/v%). Specifically, for T-AOC indicators, the ratio used was 1:4 (v/v%). After centrifugation to remove

debris, supernatants were collected. Absorbance values for MDA, T-AOC, CAT, and GSH indicators were measured at 532 nm, 593 nm, 405 nm, and 420 nm, respectively, using enzyme-linked assay kits following their instructions. The biochemical assay kits were purchased from Nanjing Jiancheng Bioengineering Institute, with the following catalog numbers: MDA assay kit (A003-1-2), CAT assay kit (A007-2-1), T-AOC assay kit (A015-2-1), GSH assay kit (A006-2-1).

## 2.13. CCK8 assay

10  $\mu$ L of CCK-8 reagent (Biosharp, BS350B) was added to BV-2 cells stimulated with different concentrations (0, 0.1, 1, 10, 100, 1000  $\mu$ M) of Mon (F. Jiang et al., 2020). The cells were then incubated at 37 °C for 2 h. Subsequently, absorbance was measured at 450 nm wavelength using a microplate reader to calculate cell viability.

## 2.14. Heat stability assay

BV-2 cells were split into control and Mon (100  $\mu$ M) treated groups. After 24 h, cells were collected in PBS with protease inhibitors and heated at temperatures from 40 °C to 64 °C for 3 min in 9 EP tubes. They were then cooled and incubated overnight at -80 °C, repeating this cycle 3 times. Samples were boiled with 6  $\times$  protein loading buffer for Western blotting to detect MMP9 expression.

## 2.15. Enzymatic stability assay

$1 \times 10^7$  BV-2 cells were lysed in 1 mL RIPA lysis buffer (Solarbio, Beijing) with Oprotease and phosphatase inhibitors on ice for 30 min. After centrifugation, the supernatant was collected. Protein concentration was measured with the BCA method (Beyotime) and adjusted to 5  $\mu$ g/ $\mu$ L. Samples were divided into 6 aliquots (20  $\mu$ L each). Four aliquots were incubated overnight at 4 °C with Monotropine (4, 8, 16, and 32  $\mu$ M). A 1:1000 dilution of chymotrypsin (Merck, USA) was added to experimental samples; controls had no proteinase E. After 30 min at room temperature, the reaction was stopped with 6  $\times$  protein loading buffer and samples were boiled. MMP9 expression was detected by Western blot.

## 2.16. MMP9 overexpression transfection

The day before transfection, BV-2 cells were seeded in 24-well plates and cultured at 37 °C until 80 % confluent. ExFect Transfection Reagent (T101-01, Vazyme, Nanjing), pLV3-CMV-Mmp9 (mouse)-3  $\times$  FLAG-Zeo plasmid (P50330, Miaoling, Shanghai), and Opti-MEM medium were mixed in a 2  $\mu$ L: 1  $\mu$ g ratio. After incubating the mixture at room temperature for 15–20 min, it was added dropwise to the 24-well plate. The cells were cultured at 37 °C with 5 % FBS-containing medium for 6–8 h, then incubated for an additional 24 h for further experiments.

## 2.17. Real-time quantitative PCR (RT-qPCR) analysis

Cells cultured in 6-well plates or brain tissues collected were treated with Trizol reagent. 1 mL of Trizol solution was added per well/cell pellet (20 mg tissue) until complete lysis. RNA was extracted with ice-cold chloroform, precipitated with isopropanol, washed with 75 % ethanol, and finally dissolved in DEPC-treated water. Following the instructions of the third-generation reverse transcription kit (R312-01, Vazyme), 1  $\mu$ g of total RNA was reverse transcribed into cDNA using reverse transcriptase. Using the SYBR Green qPCR Premix (Q711-02, Vazyme), qPCR reactions were set up with 20-fold diluted cDNA as template in accordance with the manufacturer's protocol. The qPCR reactions were performed on an ABI 7500 instrument. Primers were designed as follows: VEGF: "F: TCACCAAGGCCAGCACATAG, R: GAGGCTCCAGGGCATTAGAC", VEGFR2: "F: CGTCAA-CAAAGTCGGGAGA, R: CAGTGCACCACAAAGACACG",  $\beta$ -actin: "F:

CCTGGCACCCAGCACAAT, R: GCTGATCCACATCTGCTGGAA" (Y. Wang et al., 2018), synthesized by Sangon Biotech. The relative expression levels of target genes were calculated using the  $2^{-\Delta\Delta Ct}$  method, with  $\beta$ -actin as the internal reference gene.

### 2.18. Molecular docking

In this study, we used Schrodinger and PyMOL software for screening MMP9 inhibitors. Monotropein's structure was obtained from PubChem, while MMP9's 3D structure (PDB code: 2ow1) was from the PDB database. Schrodinger's Maestro module handled virtual screening, and PyMOL visualized Monotropein's docking with MMP9.

### 2.19. Reactive oxygen species (ROS) measurement

Reactive oxygen species (ROS) levels were measured using DHE staining, where DHE reacts with superoxide anions to produce red fluorescence, allowing for the visualization of ROS accumulation in brain tissues. Fresh brain tissues were washed with cold PBS, rapidly frozen, and sliced into 10  $\mu$ m sections. Sections were treated with 5  $\mu$ M Dihydroethidium (DHE) at 37 °C for 30 min to detect superoxide anion levels. After washing with PBS, nuclei were stained with DAPI. ROS levels in brain tissues were observed using confocal microscopy.

### 2.20. Open field test (OFT)

The locomotor activity of mice was assessed using the OFT. Mice from each experimental group were placed in the center of a 40  $\times$  40 cm box and allowed to freely explore for 5 min. Their movement was recorded, and total distance traveled was analyzed.

### 2.21. Morris water maze experiment

The Morris water maze (MWM) test, assesses learning and memory. It includes two phases: spatial navigation and spatial probe. Over five days, mice are trained to find a hidden platform within 120 s per trial. On days 1, 4, and 7, a 60-s positioning navigation test is conducted, recording escape latency. After these tests on days 4 and 7, a spatial probe test is done without the platform, allowing mice to swim for 60 s to measure their time in the target quadrant.

### 2.22. Data analysis

All experimental data were analyzed using GraphPad Prism software (version 8.1; La Jolla, CA). Prior to analysis, Shapiro-Wilk tests were conducted using SPSS software to verify normal distribution of the data. For data conforming to normal distribution, one-way ANOVA followed by Tukey's post hoc analysis was used for comparisons among three groups, and *t*-tests were used for comparisons between two groups. For non-normally distributed data, statistical analysis was performed using

the Mann-Whitney *U* test. All data are presented as mean  $\pm$  standard error of the mean (SEM; *n* = 3 or 6). Statistical significance was set at \**P* < 0.05, \*\**P* < 0.01, \*\*\**P* < 0.001, and \*\*\*\**P* < 0.0001.

## 3. Results

### 3.1. MMP9 is highly expressed in sepsis-associated encephalopathy and is positively correlated with disease severity

The GEO database is a global repository for gene expression data (Barrett et al., 2005). In this study, dataset GSE167610 showed that MMP9 was significantly upregulated in the SAE model compared to controls (Fig. 1A). BV-2 cells stimulated with varying LPS concentrations showed increased MMP9 activity (Fig. 1B). Correlation analysis confirmed a positive relationship between MMP9 activity and LPS dosage (*r* = 0.9355, *p* < 0.0001, Fig. 1C). Using the CLP model, ELISA measurements showed significantly higher MMP9 levels in SAE mice compared to controls (Fig. 1D). These findings indicate elevated MMP9 expression in SAE.

### 3.2. MMP9 promotes the progression of sepsis-associated encephalopathy

MMP9 can degrade extracellular matrix proteins, disrupting the BBB and worsening brain tissue damage (Yu et al., 2022). This allows inflammatory cells and mediators to enter, increasing encephalitis and neuronal injury. In a co-culture model of LPS-stimulated BV-2 and HUVECs cells, we assessed TEER and tight junction protein levels in HUVECs after inhibiting MMP9 with MMP9-IN-1. MMP9 suppression was confirmed by immunofluorescence (Fig. 2A). Inhibition of MMP9 significantly reversed the LPS-induced decrease in TEER and increased tight junction proteins ZO-1, Occludin, and Claudin-5, compared to the LPS group (Fig. 2B–F). MMP9 also promotes inflammatory responses in neurons and glial cells (Yu et al., 2022). Immunofluorescence showed fewer Iba-1-positive cells in BV-2 cells after MMP9 inhibition, indicating reduced neuroinflammatory cell activation (Fig. 2G).

VEGF increases angiogenesis and vascular permeability by binding to VEGFR2. In septic encephalopathy, inflammation increases cytokine production, raising VEGF levels and VEGFR2 activation, which disrupts the BBB and increases brain inflammation and damage (Ding et al., 2023). MMP9 inhibition significantly reduced VEGF and VEGFR2 levels in HUVECs, compared to the LPS group (Fig. 2H–K). MMP9 expression was significantly upregulated in the SAE model, and this was closely associated with key pathological features including BBB disruption, neuroinflammation, and microvascular hyperpermeability. Mechanistically, MMP9 contributed to the degradation of tight junction proteins (ZO-1, Occludin, Claudin-5), activation of microglia (as indicated by increased Iba-1+ staining), and upregulation of the VEGF/VEGFR2 signaling pathway. These findings suggest that MMP9 actively promotes the progression of SAE by exacerbating vascular dysfunction and inflammatory responses. In summary, blocking MMP9 alleviates BBB

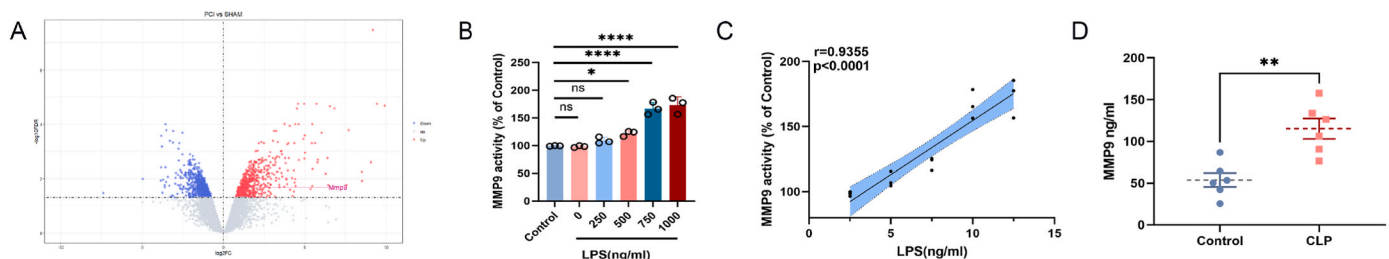


**Fig. 1.** Correlation analysis of MMP9 in SAE. A) Differential gene expression analysis of dataset GSE167610 from the GEO database. B) Effect of LPS (1–1000 ng/mL) on MMP9 activity in BV-2 cells after 24 h. C) Correlation analysis between MMP9 activity and increasing doses of LPS. D) ELISA detection of MMP9 content in brain tissue homogenates. Data were analyzed by one-way ANOVA and presented as mean  $\pm$  SEM (*n* = 6). Tukey's post-hoc analysis was used to compare the differences between each group. ns indicates *p* > 0.05, \*, \*\*, \*\*\*, \*\*\*\* represent *p* < 0.05, *p* < 0.01, *p* < 0.001, *p* < 0.0001, respectively, indicating significant differences. (Result of one-way analysis of variance (ANOVA) *F* (5, 12) = 49.91, *P* < 0.0001, Fig. 1B. Result of unpaired Student's *t*-test *t* (10) = 4.147, *P* = 0.0020, Fig. 1D).

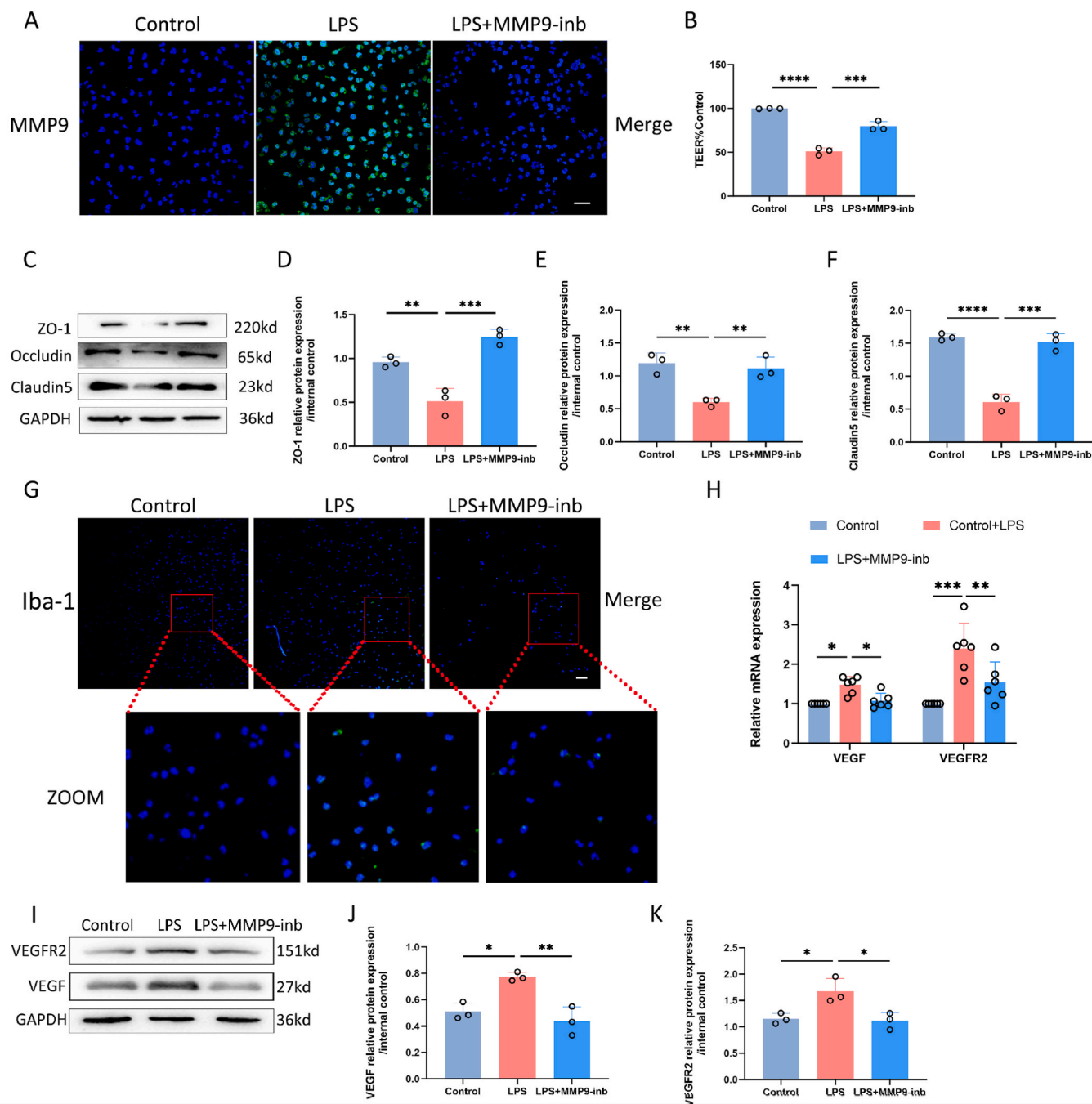


**Fig. 2.** MMP9's role in septic encephalopathy. A) MMP9 immunofluorescence in BV-2 cells (scale bar: 200 μm). B) TEER measurement in HUVECs. C) Western blot of tight junction proteins in HUVECs. D-F) Grayscale analysis of (C). G) Iba-1 immunofluorescence in BV-2 cells (scale bar: 100 μm). H) Transcriptional detection of VEGF and VEGFR2 in HUVECs. I) Western blot of VEGF and VEGFR2 in HUVECs. J-K) Grayscale analysis of (I). Data: one-way ANOVA, mean ± SEM (n = 6). Tukey's post-hoc: \*, \*\*, \*\*\*, \*\*\*\* indicate significant differences ( $p < 0.05$ ,  $p < 0.01$ ,  $p < 0.001$ ,  $p < 0.0001$ ), ns indicates  $p > 0.05$ . (Results of one-way analysis of variance (ANOVA) F (2, 6) = 120.8,  $P < 0.0001$ , Fig. 2B; F (2, 6) = 37.23,  $P = 0.0004$ , Fig. 2D; F (2, 6) = 16.35,  $P = 0.0037$ , Fig. 2E; F (2, 6) = 81.72,  $P < 0.0001$ , Fig. 2F; F (2, 6) = 16.32,  $P = 0.0037$ , Fig. 2J; F (2, 6) = 9.044,  $P = 0.0155$ , Fig. 2K. Results of unpaired student's t-test VEGF:control vs control + lps  $t(7) = 3.638$ ,  $P = 0.0160$ , Fig. 2H; control + lps vs lps + MMP9-inb  $t(10) = 3.380$ ,  $P = 0.0139$ , Fig. 2H. Results of two-way analysis of variance VEGFR2 F (1, 12) = 8.343,  $P = 0.0136$ ; F (2, 12) = 15.03,  $P = 0.0005$ , Fig. 2H).

disruption, neuroinflammatory responses, angiogenesis, and vascular permeability in septic encephalopathy.

### 3.3. Monotropein can bind to the target protein MMP9

Visualizing drug-target interactions in 3D helps us understand their spatial conformation, interactions, and binding sites, aiding in

evaluating binding stability and affinity. In Fig. 3A, we show the 3D docking results between Mon and MMP9, with a docking score of -6.16. The binding sites identified are PRO-421, PHE-110, GLR-402, and GLY-186. To validate these results, we conducted thermal and enzymatic stability analyses of MMP9 with Mon. The CCK-8 assay determined that Mon concentrations up to 100 μM were safe for BV-2 cells. Thus, 100 μM was used for further experiments (Fig. S1). The thermal stability

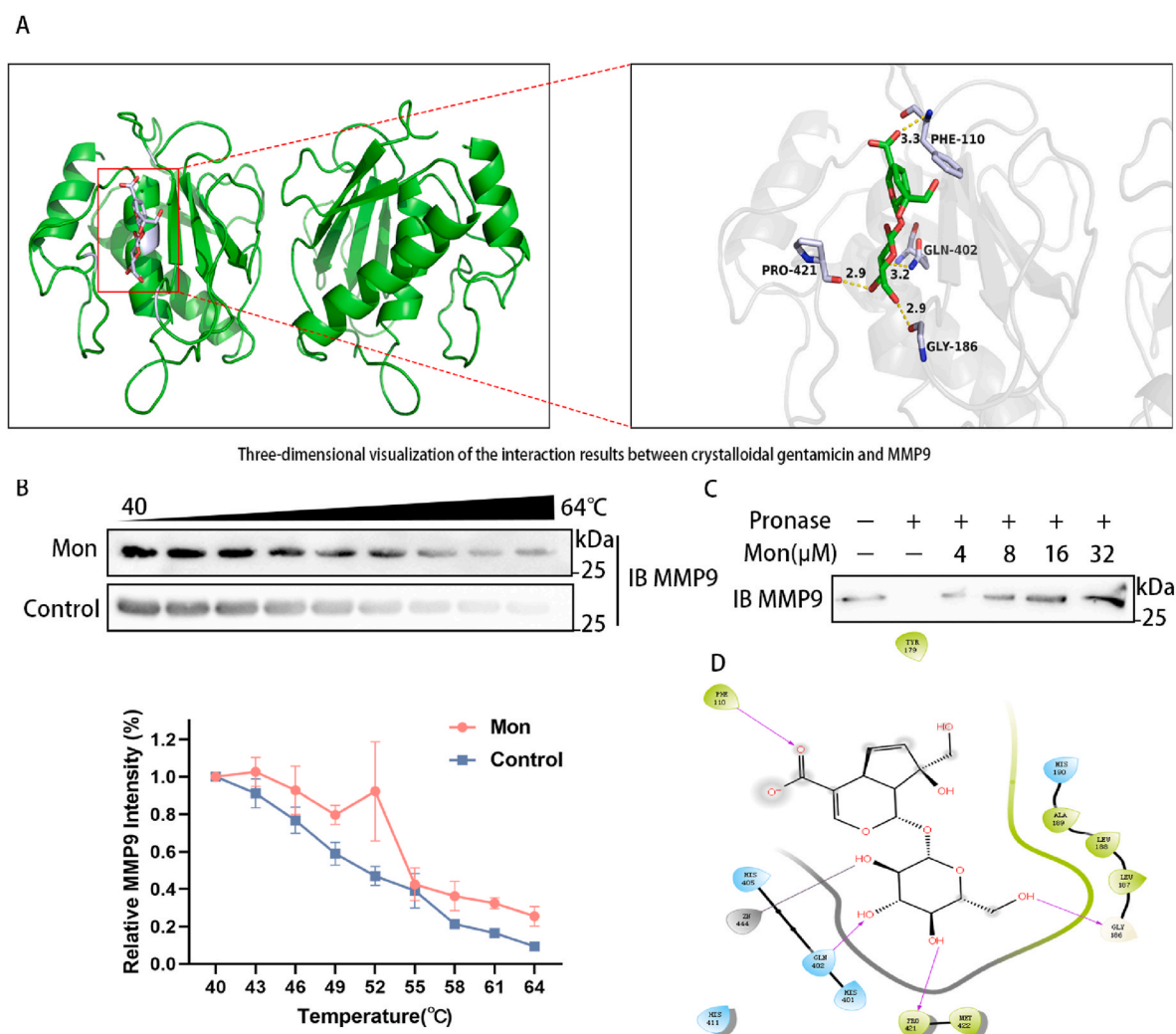


**Fig. 3.** Molecular Docking of MMP9 Protein Structure with Monotropein and Thermal Stability and Enzymatic Stability Experiments of Monotropein with Target MMP9 Protein. A) The visualization results of the virtual docking between monotropein and MMP9. B) Thermal stability experiment. C) Enzymatic stability experiment. D) Conformation of MMP9-Mon complex.

experiment (Fig. 3B) showed that Mon significantly increased MMP9's stability at temperatures from 40 °C to 64 °C. Enzymatic stability tests (Fig. 3C) showed that while MMP9 was degraded by protease, Mon dose-dependently enhanced MMP9 stability against degradation. Finally, we presented the 2D conformation of the Monotropein-MMP9 complex (Fig. 3D).

### 3.4. Monotropein exerts its anti-inflammatory effects, improves vascular permeability, and protects the barrier function by targeting MMP9

We validated monotropein binding to MMP9 using molecular docking. To analyze monotropein's effects through MMP9 in SAE, we used a co-culture model of BV-2 and HUVECs cells with MMP9 overexpression. Immunofluorescence showed increased MMP9 levels in overexpressing BV-2 cells, which monotropein reduced (Fig. 4A). We measured TEER and tight junction proteins (ZO-1, Occludin, Claudin-5) in co-cultured HUVECs to see if monotropein protects BBB integrity through MMP9. Monotropein significantly improved TEER and tight junction protein expression compared to MMP9 overexpression alone (Fig. 4B–F). Notably, the variability in TEER measurements among different groups may reflect individual differences in BBB integrity and response to treatment, which is common in complex biological systems. Microglial polarization was assessed using the activation marker Iba-1. Monotropein reversed the polarization induced by MMP9 overexpression

(Fig. 4G). Lastly, we measured VEGF and VEGFR2 levels in HUVECs to assess microvascular permeability. Monotropein treatment significantly reduced VEGFR2 protein expression in HUVECs compared to the LPS + OE-MMP9 group ( $p < 0.01$ ). Specifically, VEGFR2 levels were markedly lower in the LPS + MON group compared to both the LPS and LPS + OE-MMP9 groups, indicating a potent inhibitory effect of Monotropein on VEGFR2 upregulation (Fig. 4J). Similarly, Monotropein effectively decreased VEGF protein expression in HUVECs. The LPS + MON group showed significantly lower VEGF levels compared to the LPS and LPS + OE-MMP9 groups ( $p < 0.05$ ), highlighting Monotropein's role in suppressing VEGF induction (Fig. 4K). Monotropein significantly reduced the VEGF and VEGFR2 levels elevated by MMP9 overexpression, suggesting it improves vascular permeability through MMP9 (Fig. 4H–K).

### 3.5. Monotropein can alleviate CLP-induced brain tissue damage, blood-brain barrier disruption, synaptic loss, and oxidative stress, thereby restoring cognitive function in mice

Histopathological analysis of CLP-treated brain tissues showed severe inflammation, neuronal necrosis, and disorganized cells. However, Monotropein treatment after CLP surgery normalized neuronal morphology, reduced necrosis, improved cell arrangement, and attenuated inflammation. (Fig. 5A and B). Evan's blue staining revealed significant BBB disruption in CLP mice, whereas Monotropein preserved

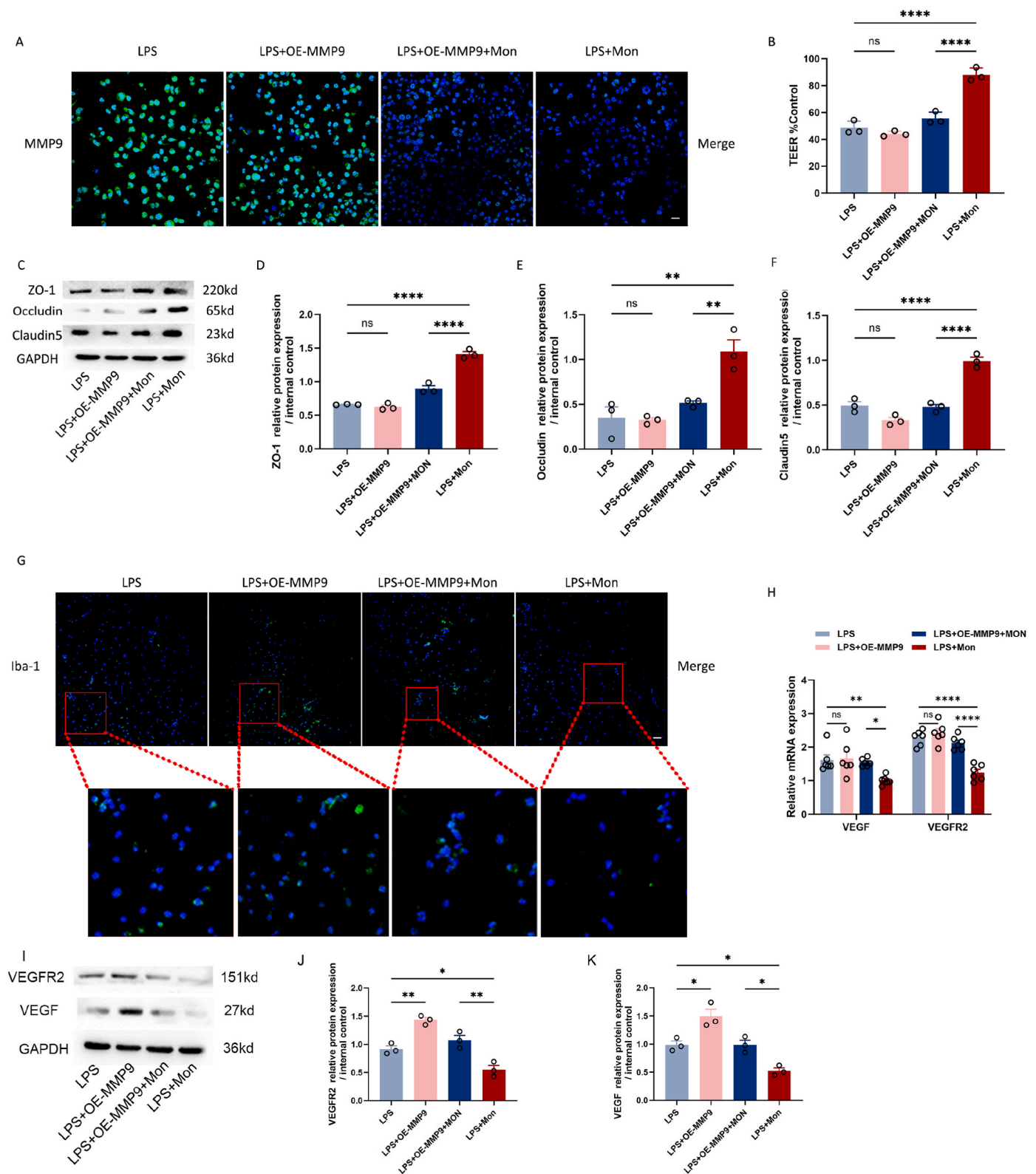
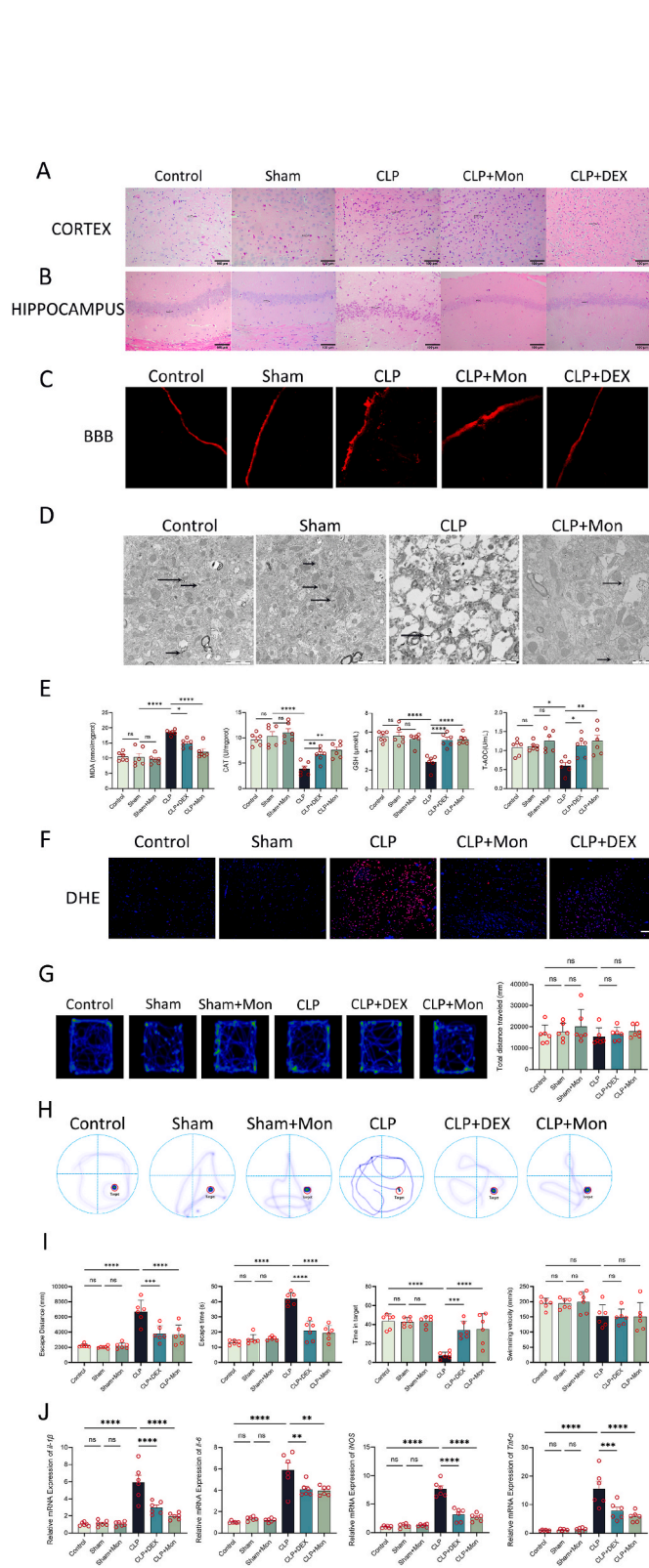


**Fig. 4.** Monotropein exerts its pharmacological effects through MMP9. A) MMP9 immunofluorescence in BV-2 cells transfected with pLV3-CMV-Mmp9 (mouse)-3 × FLAG-Zeo plasmid (scale bar: 200 μm). B) Transendothelial electrical resistance (TEER) in HUVECs. C) Western Blot of tight junction proteins in HUVECs. D-F) Grayscale analysis of (C). G) Iba-1 immunofluorescence in BV-2 cells (scale bar: 100 μm). H) Transcriptional detection of VEGF and VEGFR2 in HUVECs. I) Western Blot of VEGF and VEGFR2 in HUVECs. J-K) Grayscale analysis of (I). Data: one-way ANOVA, mean ± SEM (n = 3). Tukey's post-hoc: \*, \*\*, \*\*\*, \*\*\*\* indicate  $p < 0.05$ ,  $p < 0.01$ ,  $p < 0.001$ ,  $p < 0.0001$ , respectively, showing significant differences. (Results of one-way analysis of variance (ANOVA)  $F(3, 8) = 62.05$ ,  $P < 0.0001$ , Fig. 4B;  $F(3, 8) = 122.9$ ,  $P < 0.0001$ , Fig. 4D;  $F(3, 8) = 57.00$ ,  $P < 0.0001$ , Fig. 4E;  $F(3, 8) = 15.53$ ,  $P = 0.0011$ , Fig. 4F;  $F(3, 8) = 29.53$ ,  $P = 0.0001$ , Fig. 4J;  $F(3, 8) = 21.53$ ,  $P = 0.0003$ , Fig. 4K; Results of two-way analysis of variance  $F(3, 40) = 1.886$ ,  $P = 0.1475$ , Fig. 5H;  $F(1, 40) = 44.47$ ,  $P < 0.0001$ , Fig. 5H;  $F(3, 40) = 24.47$ ,  $P < 0.0001$ , Fig. 5H.).



(caption on next column)

**Fig. 5.** Monotropein Alleviates CLP-Induced Mouse Brain Injury. CLP was used to create a mouse SAE model. Mice were treated with Monotropein (Mon), with Dex as a positive control and Sham as a negative control. A-B) H&E-stained cerebral cortex and hippocampal CA1 sections (scale bar = 100  $\mu$ m). Black arrows indicate inflammatory cells. C) Evan's blue dye fluorescent staining (scale bar = 100  $\mu$ m). D) TEM of neuronal synapses (scale bar = 2  $\mu$ m). Black arrows denote synapses. E) Measurements of lipid peroxidation, antioxidant enzyme activity, and total antioxidant capacity in brain tissue. F) ROS detection in frozen brain sections (scale bar = 100  $\mu$ m). G) Open field test tracks and total distance traveled. H-I) Morris water maze test tracks, time in target quadrant, escape latency, distance, and velocity. J) qPCR detection of IL-1 $\beta$ , IL-6, iNOS and TNF- $\alpha$  mRNA levels. Data were analyzed by one-way ANOVA and shown as mean  $\pm$  SEM (n = 3 or 6). Tukey's post-hoc analysis compared group differences. Significance levels: ns (p > 0.05), \*, \*\*, \*\*\*, \*\*\*\* (p < 0.05, p < 0.01, p < 0.001, p < 0.0001). (Results of one-way analysis of variance (ANOVA) F (5, 30) = 17.37, P < 0.0001, Fig. 5E; F (5, 30) = 13.20, P < 0.0001, Fig. 5E; F (5, 30) = 19.77, P < 0.0001, Fig. 5E; F (5, 30) = 5.502, P = 0.0010, Fig. 5E; F (5, 30) = 0.6944, P = 0.6317, Fig. 5G; F (5, 30) = 21.85, P < 0.0001, Fig. 5I; F (5, 30) = 42.64, P < 0.0001, Fig. 5I; F (5, 30) = 14.78, P < 0.0001, Fig. 5I; F (5, 30) = 3.655, P = 0.0106, Fig. 5I.). (For interpretation of the references to color in this figure legend, the reader is referred to the Web version of this article.)

BBB integrity (Fig. 5C). Electron microscopy showed severe synaptic damage in CLP mice, mitigated by Monotropein (Fig. 5D). These findings suggest Monotropein protects against CLP-induced septic-associated encephalopathy by reducing BBB disruption and synaptic loss. Oxidative stress markers MDA, CAT, GSH, and T-AOC were assessed in brain tissue (Fig. 5E). CLP mice showed elevated MDA and decreased antioxidant enzyme activities compared to controls. Monotropein treatment significantly improved these markers and reduced brain ROS levels (Fig. 5F), indicating enhanced antioxidant capacity. Behavioral tests evaluated cognitive function. In the open field test, all groups exhibited similar locomotor abilities (Fig. 5G). In the Morris water maze, CLP mice showed impaired performance, spending less time in the target quadrant and struggling to find the platform. Monotropein treatment improved performance, reducing escape latency and distance and increasing time in the target quadrant (p < 0.0001), with no impact on swimming speed (Fig. 5H and I). The observed variability in behavioral outcomes among individual mice could be attributed to inherent differences in cognitive function and stress responses, which are influenced by factors such as age, sex, and baseline health status. The detection of inflammatory factors such as TNF- $\alpha$ , IL-1 $\beta$ , IL-6, and iNOS also indicated the anti-inflammatory effect of Monotropein (Fig. 5J). These results demonstrate Monotropein's effectiveness in alleviating CLP-induced cognitive dysfunction in mice.

#### 4. Discussion

MMP9, crucial for inflammation and tissue repair (Sunny et al., 2024), was the focus of this study on its role in septic-associated encephalopathy. Using the GEO database, we found MMP9 upregulation in septic patients, consistent with previous studies (W. Zhang, 2024). Experimental validation using GSE167610 further linked MMP9 with sepsis severity. Our analyses underscored MMP9's significant upregulation in sepsis, linking it with disease severity and guiding further research. We used an *in vitro* blood-brain barrier model to study MMP9's involvement in septic brain injury mechanisms.

Given that sepsis-associated encephalopathy (SAE) is characterized by blood-brain barrier disruption, neuroinflammation, and angiogenesis (Yue et al., 2025), we employed MMP9 inhibitors to further examine their impact on these phenotypes. This approach was chosen based on previous studies indicating the significant role of MMP9 in these pathological processes (Hu et al., 2024). In septic brain injury, MMP9 inhibitors were effective in reducing blood-brain barrier disruption, neuroinflammation, and angiogenesis. They lowered barrier permeability and inflammatory mediator infiltration, protecting neurons and brain tissues. By targeting VEGF and VEGFR2, key in angiogenesis and

vascular permeability, MMP9 inhibitors helped alleviate vascular lesions and preserve brain integrity (Tsai et al., 2022; Wu et al., 2022). These results highlight MMP9's significance in septic brain injury and the potential of MMP9 inhibitors for therapeutic intervention.

This study focused on how the drug Mon interacts with MMP9, a protein involved in various physiological and pathological processes such as tissue regeneration and tumor development (Huang, 2018). Targeting MMP9 is clinically important, and Mon showed potential therapeutic effects in this regard. The research visualized the three-dimensional binding of Mon to MMP9, revealing their spatial interactions and binding mechanisms. Thermal and enzymatic stability assays confirmed Mon's ability to stabilize MMP9 and protect it from enzyme degradation, providing structural insights. Validation in disease models using immunofluorescence and protein analysis further supported Mon as a potential therapeutic inhibitor of MMP9.

Sepsis is a major public health concern. CLP-induced sepsis in mice is a widely used model for studying therapeutic approaches (Dejager et al., 2011). HUVEC cells are validated for creating *in vitro* blood-brain barrier models (C. Liu et al., 2023). Monotropein, derived from *Gastrodia elata*, has anti-inflammatory and antioxidant properties (Y. Zhang et al., 2020). Previous studies confirmed the safety of 20 mg/kg/day of Monotropein in mice (Guo et al., 2024). In this study, we investigated Monotropein's protective effects in CLP and LPS-induced septic-associated encephalopathy (SAE). Our findings *in vivo* showed improved brain tissue pathology with Monotropein treatment.

Synaptic neuronal injury and BBB disruption are crucial in septic-associated encephalopathy (SAE) (Gofton and Young, 2012). During sepsis, inflammatory mediators and immune activation can damage synaptic neurons, causing cognitive decline (J. Jiang et al., 2023; Mazeraud et al., 2020). BBB disruption allows inflammatory mediators easier access to brain tissue, worsening inflammation and damage in SAE (Peng et al., 2021). Preserving synaptic neuronal integrity and BBB function is vital for treating SAE. Monotropein treatment in our CLP-induced sepsis model showed significant reductions in synaptic damage and restored BBB integrity, suggesting it as a potential natural therapy for sepsis-related multi-organ dysfunction.

During sepsis, the body releases inflammatory cytokines like TNF- $\alpha$ , IL-1 $\beta$ , and IL-6, triggering systemic inflammation affecting the central nervous system (Xin et al., 2023). These cytokines contribute to neuroinflammation, brain tissue damage, and increased vascular permeability (S. Gao et al., 2023; Ferreira et al., 2024). Monotropein treatment in mice enhanced antioxidant enzyme activity and reduced ROS levels in the cerebral cortex and hippocampus, highlighting its potential in mitigating septic brain injury.

Cognitive function is closely tied to septic-associated encephalopathy (SAE). Patients with sepsis often experience cognitive impairment, including decreased attention, memory loss, and slowed thinking (Tauber et al., 2021; Ling et al., 2023). BBB disruption can worsen brain injury by allowing more inflammatory mediators into brain tissue (Xin et al., 2023). Monotropein treatment in mice significantly improved learning and memory deficits caused by sepsis in behavioral tests like the Morris water maze.

In summary, this study underscores MMP9's role in septic encephalopathy using animal and cell models. MMP9 inhibitors are validated as potential treatments for septic brain injury. Research on Monotropein's interaction with MMP9 supports its potential as an MMP9 inhibitor, offering insights for drug development. Monotropein's effects in reducing oxidative stress and inflammation suggest it could effectively prevent septic encephalopathy.

## 5. Limitations

Multiple signaling pathways—such as NF- $\kappa$ B, MAPK, and Wnt/ $\beta$ -catenin—play key roles in modulating inflammation, maintaining endothelial integrity, and supporting neuronal survival. These pathways may interact with one another and could play a role in mediating the

pathological effects driven by MMP9 in the brain. Given this complexity, our future work will focus on systematically examining how MMP9 influences these signaling cascades and the crosstalk between them in the context of sepsis-associated encephalopathy. A deeper understanding of the regulatory network centered on MMP9 and its downstream targets may offer new insights into disease mechanisms and identify potential therapeutic targets.

## CRediT authorship contribution statement

**Yue Xin:** Writing – original draft, Methodology, Formal analysis, Data curation. **Tianyue Guan:** Validation, Investigation, Formal analysis, Data curation. **Guanglu Wang:** Software, Resources, Investigation. **Yannan Xiang:** Writing – review & editing, Supervision. **Mengxin Li:** Supervision, Methodology, Formal analysis. **Yikun Zhao:** Validation, Data curation. **Panpan Zhao:** Writing – review & editing, Validation, Project administration, Funding acquisition, Conceptualization.

## Funding

The authors thank the Medical Research Project of Jiangsu Provincial Health Commission (No. H2023145), and the Jiangsu Science and Technology Association Youth Science and Technology Talent Lifting Project (No. TJ-2023-058) for financial support. The funders had no role in study design, data collection and analysis, decision to publish, or preparation of the manuscript.

## Declaration of competing interest

The authors declare that they have no known competing financial interests or personal relationships that could have appeared to influence the work reported in this paper.

## Acknowledgements

The authors thank all participants of this study.

## Appendix A. Supplementary data

Supplementary data to this article can be found online at <https://doi.org/10.1016/j.neuropharm.2025.110636>.

## Data availability

No data was used for the research described in the article.

## References

- Augoff, K., Hryniewicz-Jankowska, A., Tabola, R., Stach, K., 2022. MMP9: a tough target for targeted therapy for cancer. *Cancers (Basel)* 14. <https://doi.org/10.3390/cancers14071847>.
- Barrett, T., Suzek, T.O., Troup, D.B., Wilhite, S.E., Ngau, W.C., Ledoux, P., Rudnev, D., Lash, A.E., Fujibuchi, W., Edgar, R., 2005. NCBI GEO: mining millions of expression profiles—database and tools. *Nucleic Acids Res.* 33, D562–D566. <https://doi.org/10.1093/nar/gki022>.
- Catarina, A.V., Branchini, G., Bettoni, L., De Oliveira, J.R., Nunes, F.B., 2021. Sepsis-associated encephalopathy: from pathophysiology to progress in experimental studies. *Mol. Neurobiol.* 58, 2770–2779. <https://doi.org/10.1007/s12035-021-02303-2>.
- Dal-Pizzol, F., Rojas, H.A., dos Santos, E.M., Vuolo, F., Constantino, L., Feier, G., Pasquali, M., Comim, C.M., Petronilho, F., Gelain, D.P., Quevedo, J., Moreira, J.C., Ritter, C., 2013. Matrix metalloproteinase-2 and metalloproteinase-9 activities are associated with blood-brain barrier dysfunction in an animal model of severe sepsis. *Mol. Neurobiol.* 48, 62–70. <https://doi.org/10.1007/s12035-013-8433-7>.
- de Araújo, B.E.S., da Silva Fontana, R., de Magalhães-Barbosa, M.C., Lima-Setta, F., Paravidino, V.B., Riveiro, P.M., Pulcheri, L.B., Dos Santos Salú, M., Genuíno-Oliveira, M.B., Robaina, J.R., da Cunha, Ajla, Cruz, F.F., Rocco, P.R.M., Bozza, F.A., de Castro-Faria-Neto, H.C., Prata-Barbosa, A., 2022. Clinical features, electroencephalogram, and biomarkers in pediatric sepsis-associated encephalopathy. *Sci. Rep.* 12, 10673. <https://doi.org/10.1038/s41598-022-14853-z>.

- Dejager, L., Pinheiro, I., Dejonckheere, E., Libert, C., 2011. Cecal ligation and puncture: the gold standard model for polymicrobial sepsis? *Trends Microbiol.* 19, 198–208. <https://doi.org/10.1016/j.tim.2011.01.001>.
- Ding, S., Wang, C., Wang, W., Yu, H., Chen, B., Liu, L., Zhang, M., Lang, Y., 2023. Autocrine S100B in astrocytes promotes VEGF-dependent inflammation and oxidative stress and causes impaired neuroprotection. *Cell Biol. Toxicol.* 39, 1–25. <https://doi.org/10.1007/s10565-021-09674-1>.
- Dufour, A., Sampson, N.S., Li, J., Kuscü, C., Rizzo, R.C., Deleon, J.L., Zhi, J., Jaber, N., Liu, E., Zucker, S., Cao, J., 2011. Small-molecule anticancer compounds selectively target the hemopexin domain of matrix metalloproteinase-9. *Cancer Res.* 71, 4977–4988. <https://doi.org/10.1158/0008-5472.Can-10-4552>.
- Dumbuya, J.S., Li, S., Liang, L., Zeng, Q., 2023. Paediatric sepsis-associated encephalopathy (SAE): a comprehensive review. *Mol. Med.* 29, 27. <https://doi.org/10.1186/s10020-023-00621-w>.
- Ferreira, F.M., Gomes, S.V., Carvalho, L.C.F., de Alcantara, A.C., da Cruz Castro, M.L., Perucci, L.O., Pio, S., Talvani, A., de Abreu Vieira, P.M., Calsavara, A.J.C., Costa, D. C., 2024. Potential of piperine for neuroprotection in sepsis-associated encephalopathy. *Life Sci.* 337, 122353. <https://doi.org/10.1016/j.lfs.2023.122353>.
- Gao, Q., Hernandez, M.S., 2021. Sepsis-associated encephalopathy and blood-brain barrier dysfunction. *Inflammation* 44, 2143–2150. <https://doi.org/10.1007/s10753-021-01501-3>.
- Gao, S., Jiang, Y., Chen, Z., Zhao, X., Gu, J., Wu, H., Liao, Y., Sun, H., Wang, J., Chen, W., 2023. Metabolic reprogramming of microglia in sepsis-associated encephalopathy: insights from neuroinflammation. *Curr. Neuropharmacol.* 21, 1992–2005. <https://doi.org/10.2174/1570159x216662216162606>.
- Gofton, T.E., Young, G.B., 2012. Sepsis-associated encephalopathy. *Nat. Rev. Neurol.* 8, 557–566. <https://doi.org/10.1038/nrneurol.2012.183>.
- Guo, X., Sun, W., Zhang, B., 2024. Monotropein alleviates ovalbumin-induced asthma in mouse model by inhibiting AKT/NF- $\kappa$ B pathway. *Int. Arch. Allergy Immunol.* 185, 425–435. <https://doi.org/10.1159/000535450>.
- Hou, X., Yang, S., Yin, J., 2019. Blocking the REDD1/TXNIP axis ameliorates LPS-induced vascular endothelial cell injury through repressing oxidative stress and apoptosis. *Am. J. Physiol. Cell Physiol.* 316, C104. <https://doi.org/10.1152/ajpcell.00313.2018> c10.
- Hu, Y., Hu, X.D., He, Z.Q., Liu, Y., Gui, Y.K., Zhu, S.H., Da, X., Liu, Y.N., Liu, L.X., Shen, Q.Y., Xu, G.H., 2024. Anesthesia/surgery activate MMP9 leading to blood-brain barrier disruption, triggering neuroinflammation and POD-like behavior in aged mice. *Int. Immunopharmacol.* 135, 112290. <https://doi.org/10.1016/j.intimp.2024.112290>.
- Huang, H., 2018. Matrix Metalloproteinase-9 (MMP-9) as a cancer biomarker and MMP-9 biosensors: recent advances. *Sensors (Basel)* 18. <https://doi.org/10.3390/s18103249>.
- Ito, H., Hosomi, S., Koyama, Y., Matsumoto, H., Imamura, Y., Ogura, H., Oda, J., 2022. Sepsis-associated encephalopathy: a mini-review of inflammation in the brain and body. *Front. Aging Neurosci.* 14, 912866. <https://doi.org/10.3389/fnagi.2022.912866>.
- Ji, Y., Huang, W., Chen, Y., Zhang, X., Wu, F., Tang, W., Lu, Z., Huang, C., 2023. Inhibition of MMP-2 and MMP-9 attenuates surgery-induced cognitive impairment in aged mice. *Brain Res. Bull.* 204, 110810. <https://doi.org/10.1016/j.brainresbull.2023.110810>.
- Jiang, F., Xu, X.R., Li, W.M., Xia, K., Wang, L.F., Yang, X.C., 2020. Monotropein alleviates H2O2-induced inflammation, oxidative stress and apoptosis via NF- $\kappa$ B/AP-1 signaling. *Mol. Med. Rep.* 22, 4828–4836. <https://doi.org/10.3892/mmr.2020.11548>.
- Jiang, J., Zou, Y., Xie, C., Yang, M., Tong, Q., Yuan, M., Pei, X., Deng, S., Tian, M., Xiao, L., Gong, Y., 2023. Oxytocin alleviates cognitive and memory impairments by decreasing hippocampal microglial activation and synaptic defects via OXTR/ERK/STAT3 pathway in a mouse model of sepsis-associated encephalopathy. *Brain Behav. Immun.* 114, 195–213. <https://doi.org/10.1016/j.bbi.2023.08.023>.
- Kaczmarek, K.T., Protokowicz, K., Kaczmarek, L., 2023. Matrix metalloproteinase-9: a magic drug target in neuropsychiatry? *J. Neurochem.* 168 (9), 1842–1853. <https://doi.org/10.1111/jnc.15976>.
- Li, H.R., Liu, Q., Zhu, C.L., Sun, X.Y., Sun, C.Y., Yu, C.M., Li, P., Deng, X.M., Wang, J.F., 2023.  $\beta$ -Nicotinamide mononucleotide activates NAD<sup>+</sup>/SIRT1 pathway and attenuates inflammatory and oxidative responses in the hippocampus regions of septic mice. *Redox Biol.* 63, 102745. <https://doi.org/10.1016/j.redox.2023.102745>.
- Li, Z., Li, D., Chen, R., Gao, S., Xu, Z., Li, N., 2023. Cell death regulation: a new way for natural products to treat osteoporosis. *Pharmacol. Res.* 187, 106635. <https://doi.org/10.1016/j.phrs.2022.106635>.
- Ling, J., Yu, S., Xiong, F., Li, S., 2023. HSPB8 up-regulation alleviates cognitive dysfunction in a mouse model of sepsis-associated encephalopathy. *Int. Immunopharmacol.* 122, 110448. <https://doi.org/10.1016/j.intimp.2023.110448>.
- Liu, C., Tian, Q., Wang, J., He, P., Han, S., Guo, Y., Yang, C., Wang, G., Wei, H., Li, M., 2023. Blocking P2RX7 attenuates ferroptosis in endothelium and reduces HG-induced hemorrhagic transformation after MCAO by inhibiting ERK1/2 and P53 signaling pathways. *Mol. Neurobiol.* 60, 460–479. <https://doi.org/10.1007/s12035-022-03092-y>.
- Lu, Y., Chen, Y., Li, Y., Xu, S., Lian, D., Liang, J., Jiang, D., Chen, S., Hou, S., 2023. Monotropein inhibits colitis associated cancer through VDR/JAK1/STAT1 regulation of macrophage polarization. *Int. Immunopharmacol.* 124, 110838. <https://doi.org/10.1016/j.intimp.2023.110838>.
- Lv, M., Ma, X., Zhang, K., Zhang, M., Ji, Y., Cheng, L., Shao, X., Guan, Z., Cui, J., Gao, Y., Liu, Y., Yang, Y., Liu, X., 2023. The disruption of blood-brain barrier induced by long-term arsenic exposure is associated with the increase of MMP-9 and MMP-2: the characteristics are similar to those caused by senescence. *Chem. Biol. Interact.* 385, 110743. <https://doi.org/10.1016/j.cbi.2023.110743>.
- Manabe, T., Heneka, M.T., 2022. Cerebral dysfunctions caused by sepsis during ageing. *Nat. Rev. Immunol.* 22, 444–458. <https://doi.org/10.1038/s41577-021-00643-7>.
- Mazeraud, A., Righy, C., Bouchereau, E., Benghanem, S., Bozza, F.A., Sharshar, T., 2020. Septic-associated encephalopathy: a comprehensive review. *Neurotherapeutics* 17, 392–403. <https://doi.org/10.1007/s13311-020-00862-1>.
- Mieres-Castro, D., Schmeda-Hirschmann, G., Theoduloz, C., Gómez-Alonso, S., Pérez-Navarro, J., Márquez, K., Jiménez-Aspee, F., 2019. Antioxidant activity and the isolation of polyphenols and new iridoids from Chilean Gaultheria phillyreifolia and G. poeppigii berries. *Food Chem.* 291, 167–179. <https://doi.org/10.1016/j.foodchem.2019.04.019>.
- Peng, X., Luo, Z., He, S., Zhang, L., Li, Y., 2021. Blood-brain barrier disruption by lipopolysaccharide and sepsis-associated encephalopathy. *Front. Cell. Infect. Microbiol.* 11, 768108. <https://doi.org/10.3389/fcimb.2021.768108>.
- Piva, S., Bertoni, M., Gitti, N., Rasulo, F.A., Latronico, N., 2023. Neurological complications of sepsis. *Curr. Opin. Crit. Care* 29, 75–84. <https://doi.org/10.1097/mcc.0000000000001022>.
- Ringland, C., Schweig, J.E., Eisenbaum, M., Paris, D., Ait-Ghezala, G., Mullan, M., Crawford, F., Abdullah, L., Bachmeier, C., 2021. MMP9 modulation improves specific neurobehavioral deficits in a mouse model of alzheimer's disease. *BMC Neurosci.* 22, 39. <https://doi.org/10.1186/s12868-021-00643-2>.
- Shi, J., Yu, T., Song, K., Du, S., He, S., Hu, X., Li, X., Li, H., Dong, S., Zhang, Y., Xie, Z., Li, C., Yu, J., 2021. Dexmedetomidine ameliorates endotoxin-induced acute lung injury in vivo and in vitro by preserving mitochondrial dynamic equilibrium through the HIF-1 $\alpha$ /HO-1 signaling pathway. *Redox Biol.* 41, 101954. <https://doi.org/10.1016/j.redox.2021.101954>.
- Shin, J.S., Yun, K.J., Chung, K.S., Seo, K.H., Park, H.J., Cho, Y.W., Baek, N.I., Jang, D., Lee, K.T., 2013. Monotropein isolated from the roots of Morinda officinalis ameliorates proinflammatory mediators in RAW 264.7 macrophages and dextran sulfate sodium (DSS)-induced colitis via NF- $\kappa$ B inactivation. *Food Chem. Toxicol.* 53, 263–271. <https://doi.org/10.1016/j.fct.2012.12.013>.
- Simões Da Gama, C., Morin-Brureau, M., 2022. Study of BBB dysregulation in neuropathogenicity using integrative human model of blood-brain barrier. *Front. Cell. Neurosci.* 16, 863836. <https://doi.org/10.3389/fncel.2022.863836>.
- Sun, J., Ding, X., Liu, S., Duan, X., Liang, H., Sun, T., 2020. Adipose-derived mesenchymal stem cells attenuate acute lung injury and improve the gut microbiota in septic rats. *Stem Cell Res. Ther.* 11, 384. <https://doi.org/10.1186/s13287-020-01902-5>.
- Sunny, A., James, R.R., Menon, S.R., Rayaroth, S., Daniel, A., Thompson, N.A., Tharakan, B., 2024. Matrix Metalloproteinase-9 inhibitors as therapeutic drugs for traumatic brain injury. *Neurochem. Int.* 172, 105642. <https://doi.org/10.1016/j.neuint.2023.105642>.
- Tauber, S.C., Djukic, M., Gossner, J., Eiffert, H., Brück, W., Nau, R., 2021. Sepsis-associated encephalopathy and septic encephalitis: an update. *Expert Rev. Anti Infect. Ther.* 19, 215–231. <https://doi.org/10.1080/14787210.2020.1812384>.
- Tsai, C.Y., Wu, J.C.C., Wu, C.J., Chan, S.H.H., 2022. Protective role of VEGF/VEGFR2 signaling against high fatality associated with hepatic encephalopathy via sustaining mitochondrial bioenergetics functions. *J. Biomed. Sci.* 29, 47. <https://doi.org/10.1186/s12929-022-00831-0>.
- Wang, C., Mao, C., Lou, Y., Xu, J., Wang, Q., Zhang, Z., Tang, Q., Zhang, X., Xu, H., Feng, Y., 2018. Monotropein promotes angiogenesis and inhibits oxidative stress-induced autophagy in endothelial progenitor cells to accelerate wound healing. *J. Cell Mol. Med.* 22, 1583–1600. <https://doi.org/10.1111/jcmm.13434>.
- Wang, Y., Zhang, F., Wang, J., Hu, L., Jiang, F., Chen, J., Chen, J., Wang, L., 2018. lncRNA LOC100132354 promotes angiogenesis through VEGFA/VEGFR2 signaling pathway in lung adenocarcinoma. *Cancer Manag. Res.* 10, 4257–4266. <https://doi.org/10.2147/cmar.S177327>.
- Wu, M., Gong, Y., Jiang, L., Zhang, M., Gu, H., Shen, H., Dang, B., 2022. VEGF regulates the blood-brain barrier through MMP-9 in a rat model of traumatic brain injury. *Exp. Ther. Med.* 24, 728. <https://doi.org/10.3892/etm.2022.11664>.
- Wu, M., Lai, H., Peng, W., Zhou, X., Zhu, L., Tu, H., Yuan, K., Yang, Z., 2023. Monotropein: a comprehensive review of biosynthesis, physicochemical properties, pharmacokinetics, and pharmacology. *Front. Pharmacol.* 14, 1109940. <https://doi.org/10.3389/fphar.2023.1109940>.
- Xin, Y., Tian, M., Deng, S., Li, J., Yang, M., Gao, J., Pei, X., Wang, Y., Tan, J., Zhao, F., Gao, Y., Gong, Y., 2023. The key drivers of brain injury by systemic inflammatory responses after sepsis: Microglia and neuroinflammation. *Mol. Neurobiol.* 60, 1369–1390. <https://doi.org/10.1007/s12035-022-03148-z>.
- Yan, X., Yang, K., Xiao, Q., Hou, R., Pan, X., Zhu, X., 2022. Central role of microglia in sepsis-associated encephalopathy: from mechanism to therapy. *Front. Immunol.* 13, 929316. <https://doi.org/10.3389/fimmu.2022.929316>.
- Yu, Z., Fang, X., Liu, W., Sun, R., Zhou, J., Pu, Y., Zhao, M., Sun, D., Xiang, Z., Liu, P., Ding, Y., Cao, L., He, C., 2022. Microglia regulate blood-brain barrier integrity via MiR-126a-5p/MMP9 axis during inflammatory demyelination. *Adv. Sci.* 9, e2105442. <https://doi.org/10.1002/adv.202105442>.
- Yue, J., Mo, L., Zeng, G., Ma, P., Zhang, X., Peng, Y., Zhang, X., Zhou, Y., Jiang, Y., Huang, N., Cheng, Y., 2025. Inhibition of neutrophil extracellular traps alleviates blood-brain barrier disruption and cognitive dysfunction via Wnt3/ $\beta$ -catenin/TCF4 signaling in sepsis-associated encephalopathy. *J. Neuroinflammation* 22 (1), 87. <https://doi.org/10.1186/s12974-025-03395-6>.
- Zhang, W., 2024. Critical roles of S100A12, MMP9, and PRNT3 in sepsis diagnosis: insights from multiple microarray data analyses. *Comput. Biol. Med.* 171, 108222. <https://doi.org/10.1016/j.combiomed.2024.108222>.
- Zhang, Y., Chen, Y., Li, B., Ding, P., Jin, D., Hou, S., Cai, X., Sheng, X., 2020. The effect of monotropein on alleviating cisplatin-induced acute kidney injury by inhibiting oxidative damage, inflammation and apoptosis. *Biomed. Pharmacother.* 129, 110408. <https://doi.org/10.1016/j.biopha.2020.110408>.